Synthesis of High-Performance Photonic Crystal Film for SERS Applications via Drop-Coating Method

Ming-Xue Wei [1], Chao-Hui Liu [2], Han Lee [3], Bo-Wei Lee [1], Chun-Han Hsu [4], Hong-Ping Lin [2,*] and Yu-Chun Wu [1,*]

[1] Department of Resource Engineering, National Cheng Kung University, Tainan 701, Taiwan;
louiswei1994@gmail.com (M.-X.W.); kmsokbgp@hotmail.com (B.-W.L.)
[2] Department of Chemistry, National Cheng Kung University, Tainan 701, Taiwan; hisarah24@gmail.com
[3] Department of Materials Science and Engineering, National Cheng Kung University, Tainan 701, Taiwan;
rick594007@hotmail.com
[4] General Education Center, National Tainan Junior College of Nursing, Tainan 700, Taiwan;
chunhanhsu@gmail.com
* Correspondence: hplin@mail.ncku.edu.tw (H.-P.L.); yuchunwu@mail.ncku.edu.tw (Y.-C.W.);
Tel.: +886-6-2757-575 (ext. 65342) (H.-P.L.); +886-6-2757-575 (ext. 62824) (Y.-C.W.)

check for
updates

Abstract: Silica nanospheres with a well-controlled particle size were prepared via a nucleation-to-growth synthesis process. A facile method is proposed for improving the self-assembly behavior of silica colloidal particles in droplet coatings by the simple controlling of the drying temperature. It is shown that a periodically arranged, opal-structured, photonic crystal film with a large area of approximately 4.0 cm^2 can be prepared, even when the particle size is up to 840 nm. When the band gap of the silica photonic crystals falls in the visible-light region, the crystals exhibit distinct structural colors. Moreover, the wavelength of the reflected light increases with an increasing particle size of silica. When the photonic band gap overlaps the wavelength of the laser source, the overall Raman spectrum intensity is significantly enhanced. Accordingly, the proposed nucleation-to-growth process and drop-coating method provides a cheap and simple approach for the manufacture of uniform sized silica and surface-enhanced Raman scattering substrates, respectively.

1. Introduction

Photonic crystals (PCs) are periodic array structures consisting of two dielectric materials. Due to their unique optical photonic band gap (PBG) properties, PCs exhibit a significant light emission enhancement effect [1]. Furthermore, three-dimensional colloidal crystals, generally referred to as opal-structured PCs [2], exhibit a distinct structural color when the PBG falls within the visible light range [3]. The term "structural color" refers to the color produced by the internal structure of the crystals. Notably, when the crystals are illuminated by different light sources with a similar spatial period and wavelength, the color produced by scattering, interference and diffraction effects does not decay over time, as in traditional pigments and dyes. This is an extremely attractive optical phenomenon with many practical applications [4]. For example, by carefully adjusting the particle size of the PCs, the crystals can be made to display different visible colors at different angles and to show a brilliant iridescent color with strong anti-light bleaching properties [5].

In recent years, PCs have been widely applied in LEDs [6,7], sensors [8–11], solar cells [12,13], lasers [14], textiles [15,16], and other fields [17–20]. The three-dimensional PCs used in such applications are generally prepared via a film growth and etching process [21,22]. However,

this process is cumbersome, expensive and time-consuming. Consequently, the feasibility for using well-dispersed colloidal particles to self-assemble into colloidal crystals has attracted great interest as a simple and low-cost alternative. Many self-assembling methods have been proposed including natural deposition [23], vertical deposition [24,25], electrophoresis [26–28], drop-coating [29,30], dip-coating [31], and isothermal induced self-assembly [32]. However, these methods still suffer the disadvantages of complex equipment requirements, processing time, and particle size limitations. As a result, rapid, low-cost and more efficient methods for the preparation of high-quality colloidal crystals are still required.

Among the various methods described above, the drop-coating method, in which a colloidal suspension is simply dropped onto a glass substrate, is one of the simplest [33]. However, the drop-coating method still has several shortcomings, including, most notably, a limited particle size and a poor coverage area. The literature contains many proposals for overcoming these limitations [34–40]. For example, Ion et al. [34] prepared high-quality, thick PCs with polystyrene and SiO_2 colloidal nanoparticles by hanging droplets on a substrate. In the present study, an isothermal heating-evaporation induced self-assembly (IHEISA) method [32] is employed to improve the uniformity of the silica-based PC film and increase the particle size through a simple control of the drying temperature during the droplet coating procedure.

In recent years, environmental pollution and pesticide residues in food have emerged as important concerns. As a result, surface-enhanced Raman scattering (SERS) has attracted growing attention as an analyte detection method for a wide variety of environmental and food samples [41,42]. However, in improving the detection performance of SERS, one of the most critical challenges is that of fabricating noble metal nanostructure substrates with a large and reproducible Raman enhancement effect over a wide sampling area using less costly, high-throughput methods. Accordingly, the present study proposes a facile method for preparing opal PCs, consisting of well-ordered silica nanospheres with good control and tunability to serve as a cheap and effective substrate for SERS applications. It is shown that through carefully controlling the drop-coating temperature, the density of the nano-sized cavities in the silica PC structure can be enhanced and the transmittance of the excitation laser through the PBG reduced, thereby increasing the intensity of the reflected Raman signal.

2. Materials and Methods

2.1. Material and Substrates

Tetraethoxysilane (TEOS) (M_w: 208.33 g/mol, CAS No. 78-10-4) was purchased from Merck, Co., Ltd. (Darmstadt, Germany). Ammonia water (M_w: 35.04 g/mol, 28 wt.%, CAS No. 1336-21-6) was purchased from Sigma-Aldrich (St. Louis, MO, USA). Ethanol (M_w: 46.07 g/mol, 95%, CAS No. 64-17-5) was purchased from Merck Millipore (Burlington, VT, USA). Slide glass was purchased from Xin-Xin Chemistry Co. Ltd. (Tainan, Taiwan). All of the chemicals were used directly without further purification. In addition, distilled water was used in all of the experiments.

2.2. Synthesis of Monodisperse SiO_2 Nanospheres

In this experiment, the monodisperse SiO_2 nanospheres were prepared by a modified Stöber method, under normal temperature and pressure conditions. In particular, 2.0 g of ammonia aqueous solution (28 wt.%) and 15.0 g of distilled water were poured into 80 ml of ethanol and stirred at 250 rpm for 5 min to produce a reaction environment for nucleation. Meanwhile, 1.49 g of TEOS was dispersed in 23.7 mL of ethanol and diluted as the nucleating agent. After mixing, the nucleating agent was poured into the reaction environment and stirred at 700 rpm for 2 h to prompt nucleation. Growth agent (8.0 mL of TEOS and 32.0 mL of EtOH) was then added to the nucleation solution to enter the growth stage and stirred for 2.5 h. The solution was centrifuged at 6000 rpm, and the product was washed twice with distilled water to remove any unreacted TEOS and residual alkali. Finally, uniform

monodisperse SiO$_2$ nanospheres were obtained by washing the product in ethanol and then drying at 70 °C for 12 h.

2.3. Surface Modification of Glass Slides

The piranha solution was prepared by slowly adding hydrogen peroxide to concentrated sulfuric acid to a final volume ratio of 2:1 (concentrated sulfuric acid to hydrogen peroxide). The glass slides were immersed in the piranha solution for 8 h for surface modification. After rinsing with deionized water, the residual water droplets were removed using a high-pressure air gun. Finally, the hydrophobicity of the slides was confirmed via contact-angle tests.

2.4. Fabrication of Colloidal Crystal Coatings

A 5.0 wt.% colloidal solution was prepared by dispersing the prepared silica nanosphere powder in water and agitating the mixture ultrasonically for 10 min. The colloidal solution was placed at room temperature for 15 min, and the precipitated agglomerate was then removed. The residual solution was analyzed using a dynamic light scattering (DLS) technique to confirm the colloidal stability and uniformity of the particle size. The colloidal particles were then self-assembled on glass substrates under a constant relative humidity of 25% and drying temperatures ranging from 25 to 55 °C to form three-dimensional PCs.

2.5. Deposition of Au Thin Film

The high density and uniformity of an Au layer coated on silica-based PC films make them suitable as SERS substrates. In this work, the experiment started with the deposition of 5.0-nm-thick Au layers via an electron beam (e-beam) evaporator (VT1-10CE, ULVAC, Tainan, Taiwan) on the thin silica-based PC films. The deposition was performed under a pressure of 6–8 × 10^{-6} torr, having a deposition rate of 0.1 Å/s.

2.6. Characterization

The polydispersity index (PDI) of the colloidal solutions was measured using DLS with a particle size analyzer (DelsaNano C, Beckman Coulter Inc, Brea, CA, USA). The morphologies of the SiO$_2$ nanospheres and PC film were characterized by scanning electron microscopy (Joel, JSM-7001F, JEOL, Ltd., Tokyo, Japan). The optical properties of the PC film were measured using a UV-vis-NIR measurement system (UV-Vis Hitachi U-4100, Hitachi, Ltd., Ibaraki, Japan). Finally, the SERS spectra of the R6G deposited on Au-coated silica-based PC films with different concentrations were acquired by Raman spectroscopy (Renishaw, Renishaw, LTD., Taichung, Taiwan).

3. Results and Discussion

3.1. Preparation of Uniform SiO$_2$ Nanospheres

The uniform-sized silica nanospheres were prepared via a nucleation-to-growth synthesis process (see Section 2.2). To control the particle size of the nanospheres, different weights of TEOS (i.e., 1.5, 2.5, 4.0, 6.0, 7.0, and 9.0 g) were added to an alkaline solution consisting of NH$_{3(aq)}$/H$_2$O/EtOH = 2.0/15.0/81.8 g. When added to the alkaline solution, the TEOS hydrolyzed and condensed to form nuclei with a nano-sized dimension. Following an appropriate nucleation time, another TEOS ethanolic solution (7.5 g of TEOS and 25.2 g of EtOH) was poured into the nuclei solution to grow the particles. As the reaction process proceeded, the suspended particles grew homogeneously on the nuclei to form SiO$_2$ nanospheres with particle sizes ranging from 190 to 316 nm, depending on the TEOS concentration (Figure 1). It was found that silica nanoparticles with a larger size could be formed by increasing the NH$_3$ weight content in the nuclei solution. In particular, when the NH$_3$ content was increased from 0.63 to 0.951 and 2.0 M for a fixed TEOS weight of 0.39 g, the particle size of the silica nanoparticles

increased from 354 to 500 and 840 nm, respectively, due to the effect of the additional ammonia in increasing the silica condensation rate, as shown in Figure 2.
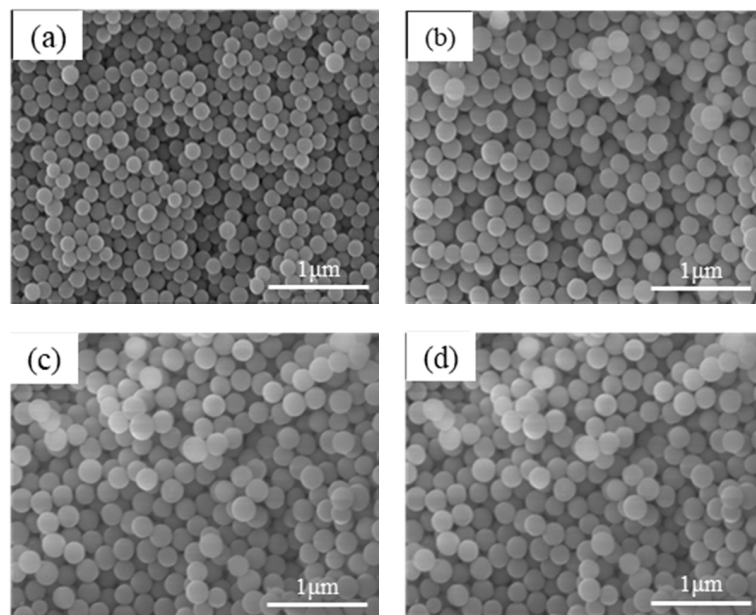

Figure 1. SEM images of SiO$_2$ nanoparticles prepared with TEOS weights of: (**a**) 1.5; (**b**) 4.0; (**c**) 6.0; and (**d**) 7.0 g.
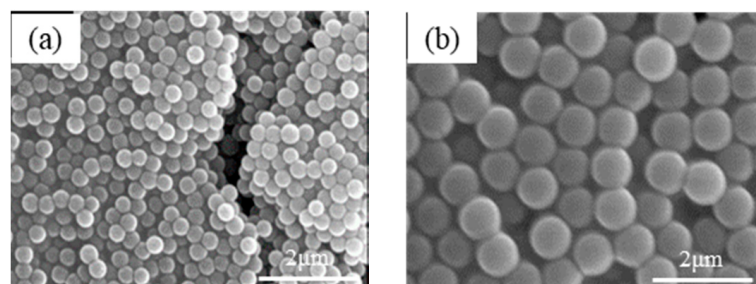
Figure 2. SEM images of enlarged SiO$_2$ nanoparticles prepared using increased NH$_{3(aq)}$ concentrations of: (**a**) 0.63 M and (**b**) 2.0 M.

In general, the uniformity and dispersity of colloidal silica particles play a key role in ensuring the formation of high-quality PCs [1–3]. In the present study, the dispersity and particle size of the colloidal silica particles were analyzed by DLS. The corresponding results are shown in Figure 3, in which all of the particle size distribution curves have the form of Gaussian distributions with a single peak and narrow width. Table 1 shows the average silica nanoparticle size and PDI of the various samples. A PDI value of less than 0.07 indicates the existence of only slight agglomerations between the particles [43]. Thus, the results presented in Table 1 confirm that the synthesis process results in the formation of a nearly monodisperse colloidal solution for the subsequent assembly of PCs.
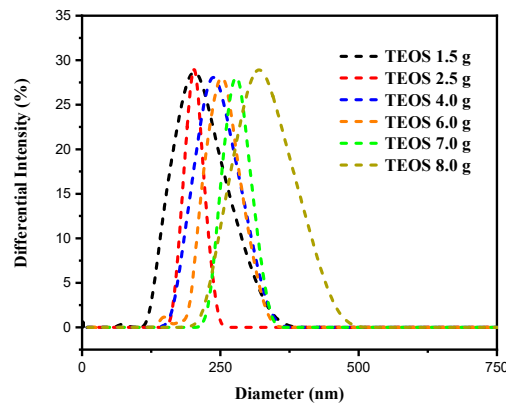
Figure 3. Dynamic light scattering (DLS) size distribution curves for colloidal silica particles prepared using different TEOS concentrations.

Table 1. Polydispersity index (PDI) and particle size distribution results obtained from DLS.

| TEOS (g)	PDI	Particle Size (nm)
1.5	0.068	190
2.5	0.001	205
4.0	0.057	239
6.0	0.007	247
7.0	0.002	279
8.0	0.040	316

3.2. Modified Drop-Coating Method Using IHEISA Approach

In the IHEISA drop-coating process, the assembling behavior and close-packing of the silica nanospheres were found to be strongly dependent on the drying temperature during the droplet coating procedure. For example, Figure 4a–c show the PC samples prepared using silica particles with a size of 500 nm at temperatures of 40, 43 and 45 °C, respectively. (Note that the relative humidity is 25% in every case). It is seen that the packing of the silica-based PCs is extremely sensitive to the drying temperature in droplet coatings. In particular, the PCs prepared at 43 °C have a more ordered packing arrangement than those prepared at either a lower or higher temperature. A similar tendency is noted for the PCs assembled from silica nanoparticles with a size of 840 nm (Figure 4d–f), for which an ordered packing arrangement is observed only for an intermediate drying temperature of 50 °C (Figure 4e). When the PCs were assembled at temperatures lower than the optimal temperature, some cubic-packing structures (indicated by the arrows in Figure 4a,d) were clearly seen. The presence of these structures indicates that the silica nanoparticles lack sufficient kinetic energy to transform from a cubic packing structure to a close-packed hexagonal structure. Conversely, at higher temperatures, the silica nanoparticles have too much kinetic energy to be trapped within the low-energy cavities of the hexagonal arrangement. Consequently, the PC samples contain a large number of structural defects, such as vacancies or dislocations, as shown in Figure 4c,f. The optimal preparation temperatures for the silica nanoparticles with a size of 500 and 840 nm are therefore 43 and 50 °C, respectively. The PC samples were also prepared using silica nanoparticles with a size of 300 and 400 nm. It was found that the optimal deposition temperatures increased with an increasing particle size of silica. In other words, the optimal deposition temperature for the preparation of well-ordered PC structures increases with an increasing silica nanoparticle size, as shown in Figure 5. Moreover, it is shown that a periodically arranged, opal-structured, photonic crystal film with a large area of approximately 4.0 cm² can be prepared, as shown in Figure S1.
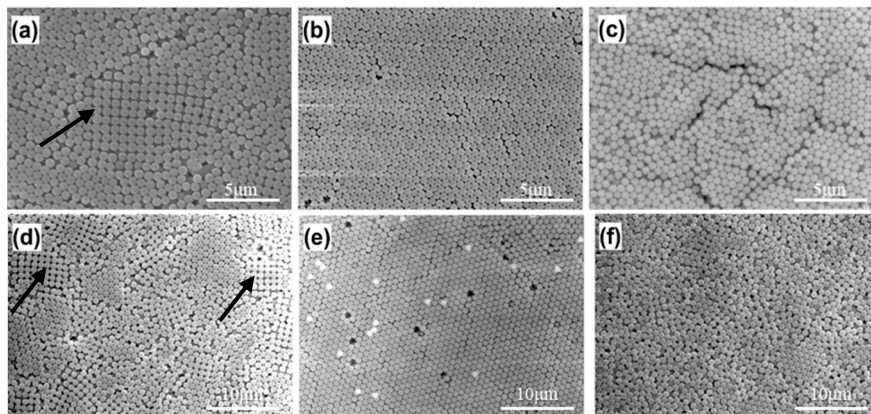
Figure 4. SEM images of photonic crystal (PC) structures prepared using 500 nm silica particles at drying temperatures of: (**a**) 40; (**b**) 43; (**c**) and 45 °C; and 840 nm silica particles at temperatures of: (**d**) 45; (**e**) 50; and (**f**) 55 °C.
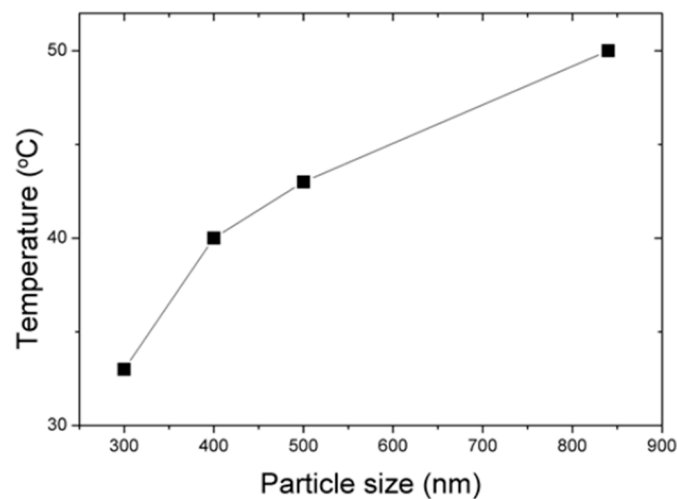
Figure 5. Optimal drying temperature in droplet coatings as a function of silica nanoparticle size.

3.3. Optical Properties of the Silica-Based PC Film

Opal photonic crystals with periodic array structures have unique optical properties of PBG properties that prevent the light of specific wavelengths from penetrating. Limited wavelengths are reflected from the structure and follow to the modified Bragg–Snell law [44,45]; the PBG wavelength can be calculated as:

$$\lambda = 1.63 \cdot a \cdot \left(n_{eff}^2 - sin^2\theta\right)^{0.5} \qquad (1)$$

where the term $1.63 \cdot a$ is the distance between the crystal planes in the (111) direction in the close-packing structure, and a is the size of the nanospheres in the PC. Moreover, λ is the wavelength of the PBG, θ is the angle of the incident light, and n_{eff} is the effective refractive index of the two different constituents of the PC (i.e., silica and air) [46], and can be calculated as:

$$n_{eff}^2 = f \cdot n_{material}^2 + (1 - f) \cdot n_{void}^2 \qquad (2)$$

Figure 6 shows the structural color of the PC films composed of silica nanospheres with a size of 180 to 310 nm. It is seen that as the particle size increases, the color changes from violet (181 nm) to lavender (199 nm), blue (231 nm), green (242 nm), yellow (271 nm), and red (310 nm), as a result of Bragg diffraction. For each film, the different layers comprise particles of the same size and have the

same thickness. As a result, an equal thickness interference phenomenon is induced, resulting in the formation of highly light-diffracting patterns [47,48].
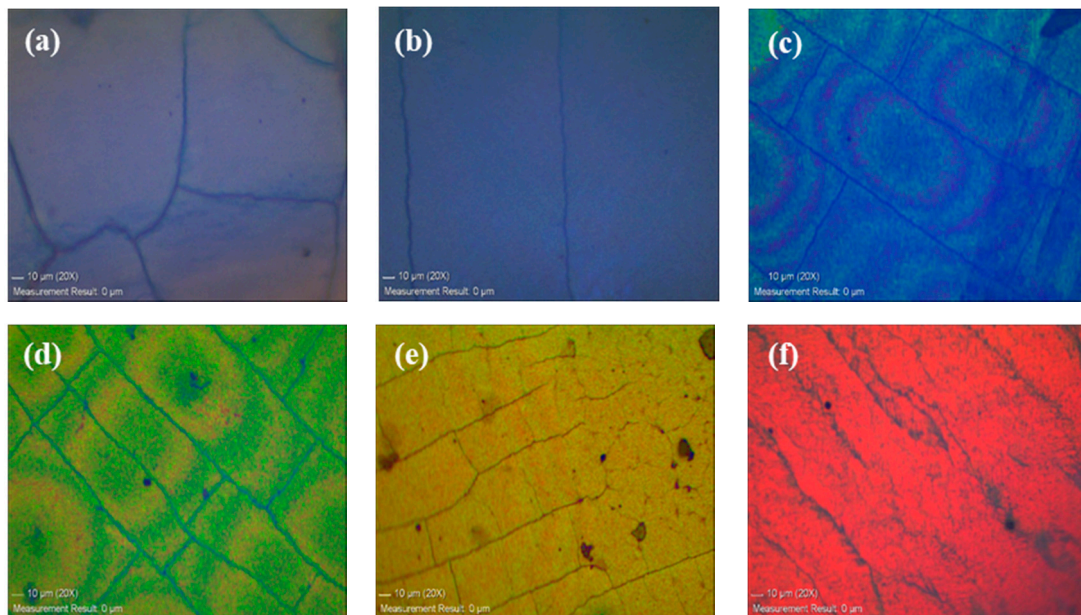
Figure 6. Optical micrographs of PC films consisting of SiO_2 spheres with dimensions of: (**a**) 181; (**b**) 199; (**c**) 231; (**d**) 242; (**e**) 271; and (**f**) 310 nm.

As shown in the reflection spectra in Figure 7a, the PBG of the silica-based PCs produces a red shift tendency as the particle size increases. Furthermore, the bandwidth of each spectrum is very narrow, which indicates a high assembly close-packing of the silica nanospheres. As shown in Figure 7b, and as predicted in Equation (1), the reflection wavelength of the PC films increases linearly ($R^2 = 0.99$) with an increasing particle size. Although the PCs possess grain boundaries and therefore cannot form a perfect close-packed structure, it is apparent that the IHEISA synthesis process provides a convenient approach for preparing PCs with the desired band gaps. Moreover, the wavelength positions of the PBGs, determined from the reflection spectra, are consistent with the structural color observed by the naked eye, and correspond to the wavelength range of the CIE1931 color space.
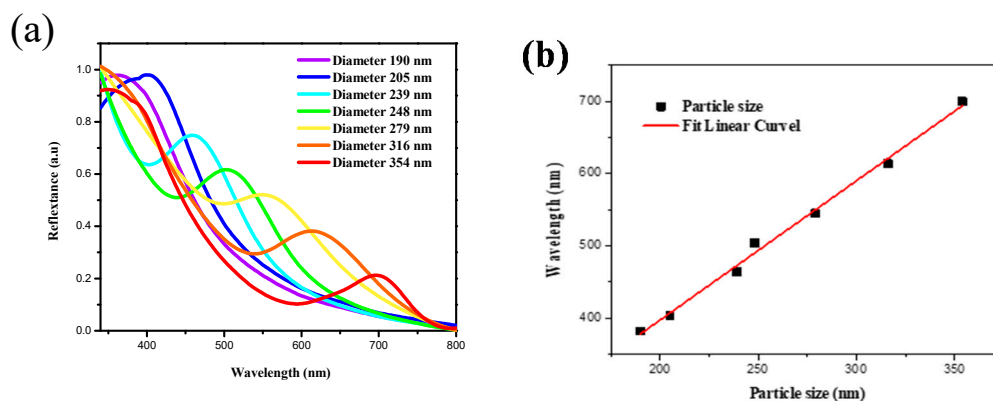

Figure 7. (**a**) Reflectance spectra of PC films consisting of SiO_2 spheres with particle dimensions between 190 and 354 nm; and (**b**) linear regression plot of photonic band gap (PBG) wavelength versus particle size.

3.4. Application of Silica-Basecd PC Films to SERS Substrates

PC films have a high density of nanosized cavities, and therefore provide an ideal substrate for the Au thin film for SERS (see Figure 8). Figure 9 shows the SERS spectra of R6G solutions of different concentrations deposited on Au-coated PC films with SiO$_2$ particle sizes of 316 (Figure 9a) and 354 nm (Figure 9b). It is seen that for the silica-based PC film with a particle size of 316 nm, the R6G detection limit is close to 1×10^{-6} M, while for the 354 nm film, the detection limit is 1×10^{-5} M. In other words, the Au-coated PC film with a silica particle size of 316 nm produces a greater Raman signal enhancement effect than the film with a particle size of 354 nm. This finding can be attributed to the fact that the PBG wavelength of the 316 nm PC film (614 nm) is close to the wavelength of the laser source (633 nm) in the Raman spectroscopy system. Thus, the likelihood of the laser beam being reflected from the film is increased, and the subsequent interaction effect between the Au hot spots and the laser therefore also increases, resulting in a greater overall Raman intensity [49]. By contrast, for the 354 nm PC film, the PBG wavelength (700 nm) is much higher than that of the laser source, and hence the enhancement effect is significantly reduced.
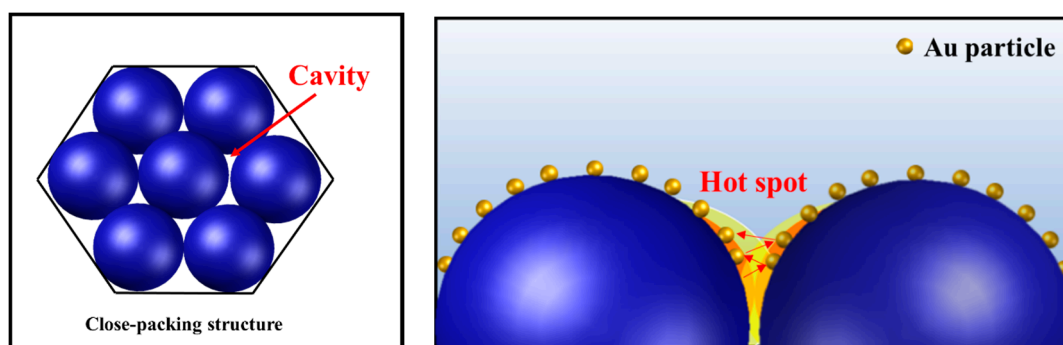
Figure 8. Silica-based PC films as a substrate for the Au thin film for surface-enhanced Raman scattering (SERS).
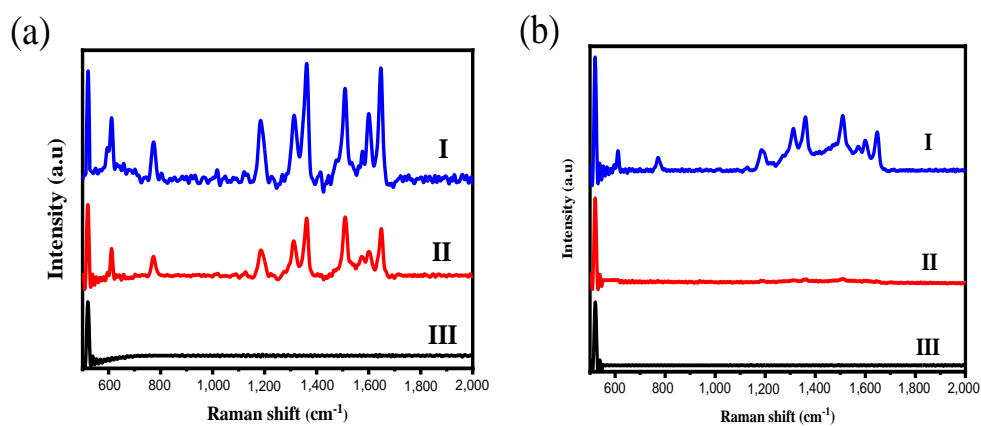
Figure 9. SERS spectra of R6G solutions with different concentrations deposited on Au-coated PC films with silica particle sizes of (**a**) 316 and (**b**) 354 nm. (I) R6G concentration 5×10^{-3} M, (II) 1×10^{-5} M, (III) 1×10^{-6} M.

4. Conclusions

A simple nucleation-to-growth synthesis method and IHEISA drop-coating technique were used to prepare PC films consisting of uniform silica nanospheres with a well-controlled particle size. It has been shown that the PC films have a tunable PBG and hence exhibit distinct structural colors. The feasibility of the silica-based PC films for SERS applications was demonstrated by depositing a

thin Au coating on the silica-based PC film surface using an E-beam evaporation technique. The results show that, given an appropriate particle size, the PBG of the PC film overlaps the wavelength of the laser source and enhances the intensity of the Raman spectrum accordingly. Thus, the proposed PC assembly method provides a low-cost and facile approach for the fabrication of SERS substrates.

Supplementary Materials: The following are available online at http://www.mdpi.com/2079-6412/10/7/679/s1, Figure S1: Photos of PC films prepared by silica with particle size of (**A**) 200 nm and (**B**) 356 nm.

Author Contributions: Conceptualization, M.-X.W., H.-P.L., and Y.-C.W.; methodology, M.-X.W., B.-W.L., and H.L.; validation, M.-X.W., C.-H.L., B.-W.L., and H.L.; formal analysis, M.-X.W., C.-H.L., and H.-L.; investigation, M.-X.W., C.-H.L., H.L. and B.-W.L.; data curation, M.-X.W. and B.-W.L.; writing—original draft preparation, M.-X.W., writing—review and editing, M.-X.W., H.-P.L., and C.-H.H.; supervision, H.-P.L., Y.-C.W., and C.-H.H. All authors have read and agreed to the published version of the manuscript.

Conflicts of Interest: The authors declare no conflict of interest.

References

1. Armstrong, E.; O'Dwyer, C. Artificial opal photonic crystals and inverse opal structures-fundamentals and applications from optics to energy storage. *J. Mater. Chem. C* **2015**, *3*, 6109–6143. [CrossRef]

2. Kin, H.N.; Yang, S. Responsive smart windows from nanoparticle-polymer composites. *Adv. Funct. Mater.* **2020**, *30*, 1902597.

3. Gao, W.; Rigout, M.; Owens, H. Self-assembly of silica colloidal crystal thin films with tunable structural colours over a wide visible spectrum. *Appl. Surf. Sci.* **2016**, *380*, 12–15. [CrossRef]

4. Wang, H.; Zhang, K.Q. Photonic crystal structures with tunable structure color as colorimetric sensors. *Sensors* **2013**, *13*, 4192–4213. [CrossRef] [PubMed]

5. Meng, Y.; Tang, B.; Ju, B.; Wu, S.; Zhang, S. Multiple colors output on voile through 3D colloidal crystals with robust mechanical properties. *ACS Appl. Mater. Interfaces* **2017**, *9*, 3024–3029. [CrossRef]

6. Li, H.; Xu, Z.; Bao, B.; Sun, N.; Song, Y. Improving the luminescence performance of quantum dot-based photonic crystals for white-light emission. *J. Mater. Chem. C* **2016**, *4*, 39–44. [CrossRef]

7. Tian, Y.; Chen, M.; Zhang, J.; Tong, Y.L.; Wang, C.F.; Wiederrecht, G.P.; Chen, S. Highly enhanced luminescence performance of LEDs via controllable layer-structured 3D photonic crystals and photonic crystal beads. *Small Methods* **2018**, *2*, 1800104. [CrossRef]

8. Hou, J.; Zhang, H.; Yang, Q.; Li, M.; Jiang, L.; Song, Y. Hydrophilic–hydrophobic patterned molecularly imprinted photonic crystal sensors for high-sensitive colorimetric detection of tetracycline. *Small* **2015**, *11*, 2738–2742. [CrossRef]

9. Zhao, X.; Xue, J.; Mu, Z.; Huang, Y.; Lu, M.; Gu, Z. Gold nanoparticle incorporated inverse opal photonic crystal capillaries for optofluidic surface enhanced Raman spectroscopy. *Biosens. Bioelectron.* **2015**, *72*, 268–274. [CrossRef]

10. Kuo, W.K.; Weng, H.P.; Hsu, J.J.; Yu, H.H. Photonic crystal-based sensors for detecting alcohol concentration. *Appl. Sci.* **2016**, *6*, 67. [CrossRef]

11. Xing, H.; Li, J.; Shi, Y.; Guo, J.; Wei, J. Thermally driven photonic actuator based on silica opal photonic crystal with liquid crystal elastomer. *ACS Appl. Mater. Interfaces* **2016**, *8*, 9440–9445. [CrossRef] [PubMed]

12. Lee, J.W.; Moon, J.H. Monolithic multiscale bilayer inverse opal electrodes for dye-sensitized solar cell applications. *Nanoscale* **2015**, *7*, 5164–5168. [CrossRef] [PubMed]

13. Yu, J.; Lei, J.; Wang, L.; Zhang, J.; Liu, Y. TiO2 inverse opal photonic crystals: Synthesis, modification, and applications—A review. *J. Alloy. Compd.* **2018**, *769*, 740–757. [CrossRef]

14. Zhao, D.; Liu, S.; Yang, H.; Ma, Z.; Reuterskiöld-Hedlund, C.; Hammar, M.; Zhou, W. Printed large-area single-mode photonic crystal bandedge surface-emitting lasers on silicon. *Sci. Rep.* **2016**, *6*, 18860. [CrossRef] [PubMed]

15. Liu, G.; Zhou, L.; Fan, Q.; Chai, L.; Shao, J. The vertical deposition self-assembly process and the formation mechanism of poly (styrene-co-methacrylic acid) photonic crystals on polyester fabrics. *J. Mater. Sci.* **2016**, *51*, 2859–2868. [CrossRef]

16. Gao, W.; Rigout, M.; Owens, H. The structural coloration of textile materials using self-assembled silica nanoparticles. *J. Nanopart. Res.* **2017**, *19*, 303. [CrossRef]

17. O'Dwyer, C. Color-coded batteries-electro-photonic inverse opal materials for enhanced electrochemical energy storage and optically encoded diagnostics. *Adv. Mater.* **2016**, *28*, 5681–5688. [CrossRef]

18. Collins, G.; Armstrong, E.; McNulty, D.; O'Hanlon, S.; Geaney, H.; O'Dwyer, C. 2D and 3D photonic crystal materials for photocatalysis and electrochemical energy storage and conversion. *Sci. Technol. Adv. Mater.* **2016**, *17*, 563–582. [CrossRef]

19. Likodimos, V. Photonic crystal-assisted visible light activated TiO$_2$ photocatalysis. *Appl. Catal. B Environ.* **2018**, *230*, 269–303. [CrossRef]

20. Chen, H.; Lou, R.; Chen, Y.; Chen, L.; Lu, J.; Dong, Q. Photonic crystal materials and their application in biomedicine. *Drug Deliv.* **2017**, *24*, 775–780. [CrossRef]

21. Kitano, K.; Suzuki, K.; Ishizaki, K.; Noda, S. Three-dimensional photonic crystals fabricated by simultaneous multidirectional etching. *Phys. Rev. B* **2015**, *91*, 155308. [CrossRef]

22. Grishina, D.A.; Harteveld, C.A.; Woldering, L.A.; Vos, W.L. Method for making a single-step etch mask for 3D monolithic nanostructures. *Nanotechnology* **2015**, *26*, 505302. [CrossRef] [PubMed]

23. Wang, L.; Wan, Y.; Li, Y.; Cai, Z.; Li, H.L.; Zhao, X.S.; Li, Q. Binary colloidal crystals fabricated with a horizontal deposition method. *Langmuir* **2009**, *25*, 6753–6759. [CrossRef]

24. Russell, J.L.; Noel, G.H.; Warren, J.M.; Tran, N.L.L.; Mallouk, T.E. Binary colloidal crystal films grown by vertical evaporation of silica nanoparticle suspensions. *Langmuir* **2017**, *33*, 10366–10373. [CrossRef]

25. Liu, G.; Zhou, L.; Wu, Y.; Wang, C.; Fan, Q.; Shao, J. The fabrication of full color P (S t-MAA) photonic crystal structure on polyester fabrics by vertical deposition self-assembly. *J. Appl. Polym. Sci.* **2015**, *132*. [CrossRef]

26. Wu, Y.; Wang, X. Rapid preparation of hexagonal and square array colloidal crystals via electrophoresis-assisted self-assembly method. *Mater. Lett.* **2015**, *142*, 109–111. [CrossRef]

27. Hung, P.S.; Liao, C.H.; Chou, Y.S.; Wang, G.R.; Wang, C.J.; Chung, W.A.; Wu, P.W. High throughput fabrication of large-area colloidal crystals via a two-stage electrophoretic deposition method. *Electrochim. Acta* **2019**, *317*, 52–60. [CrossRef]

28. Katagiri, K.; Tanaka, Y.; Uemura, K.; Inumaru, K.; Seki, T.; Takeoka, Y. Structural color coating films composed of an amorphous array of colloidal particles via electrophoretic deposition. *NPG Asia Mater.* **2017**, *9*, e355. [CrossRef]

29. Koegler, P.; Dunn, M.; Wang, P.Y.; Thissen, H.; Kingshott, P. A novel approach to quantitatively assess the uniformity of binary colloidal crystal assemblies. *Crystals* **2016**, *6*, 84. [CrossRef]

30. Huang, D.; Zeng, M.; Wang, L.; Zhang, L.; Cheng, Z. Biomimetic colloidal photonic crystals by coassembly of polystyrene nanoparticles and graphene quantum dots. *RSC Adv.* **2016**, *8*, 34839–34847. [CrossRef]

31. Nagao, D.; Kameyama, R.; Matsumoto, H.; Kobayashi, Y.; Konno, M. Single- and multi-layered patterns of polystyrene and silica particles assembled with a simple dip-coating. *Colloids Surf. A Physicochem. Eng. Asp.* **2008**, *317*, 722–729. [CrossRef]

32. Jiang, Q.; Li, C.; Shi, S.; Zhao, D.; Xiong, L.; Wei, H.; Yi, L. Assembling ultra-thick and crack-free colloidal crystals via an isothermal heating evaporation induced self-assembly method. *J. Non Cryst. Solids* **2012**, *358*, 1611–1616. [CrossRef]

33. Dalmis, R.; Birlik, I.; Azem NF, A.; Çelik, E. Modification of the sedimentation method for PMMA photonic crystal coatings. *Colloids Surf. A Physicochem. Eng. Asp.* **2019**, *577*, 194–201. [CrossRef]

34. Sandu, I.; Dumitru, M.; Fleaca, C.T.; Dumitrache, F. Hanging colloidal drop: A new photonic crystal synthesis route. *Photonics Nanostruct.* **2018**, *29*, 42–48. [CrossRef]

35. Yan, J.; Bloom, M.; Bae, S.C.; Luijten, E.; Granick, S. Linking synchronization to self-assembly using magnetic Janus colloids. *Nature* **2012**, *491*, 578–581. [CrossRef]

36. Wong, S.; Kitaev, V.; Ozin, G.A. Colloidal crystal films: Advances in universality and perfection. *J. Am. Chem. Soc.* **2003**, *125*, 15589–15598. [CrossRef]

37. Jiang, P.; McFarland, M.J. Large-scale fabrication of wafer-size colloidal crystals, macroporous polymers and nanocomposites by spin-coating. *J. Am. Chem. Soc.* **2004**, *126*, 13778–13786. [CrossRef]

38. You, B.; Wen, N.; Shi, L.; Wu, L.; Zi, J. Facile fabrication of a three-dimensional colloidal crystal film with large-area and robust mechanical properties. *J. Mater. Chem.* **2009**, *19*, 3594–3597. [CrossRef]

39. Zhang, J.; Wang, M.; Ge, X.; Wu, M.; Wu, Q.; Yang, J.; Liu, N. Facile fabrication of free-standing colloidal-crystal films by interfacial self-assembly. *J. Colloid Interface Sci.* **2011**, *353*, 16–21. [CrossRef] [PubMed]

40. Wang, J.; Wen, Y.; Feng, X.; Song, Y.; Jiang, L. Control over the wettability of colloidal crystal films by assembly temperature. *Macromol. Rapid Commun.* **2006**, *27*, 188–192. [CrossRef]

41. Jiang, Y.; Sun, D.W.; Pu, H.; Wei, Q. Surface enhanced Raman spectroscopy (SERS): A novel reliable technique for rapid detection of common harmful chemical residues. *Trends Food Sci. Technol.* **2018**, *75*, 10–22. [CrossRef]

42. Zhang, Y.; Wang, Z.; Wu, L.; Pei, Y.; Chen, P.; Cui, Y. Rapid simultaneous detection of multi-pesticide residues on apple using SERS technique. *Analyst* **2014**, *20*, 5148–5154. [CrossRef] [PubMed]

43. Hughes, J.M.; Budd, P.M.; Tiede, K.; Lewis, J. Polymerized high internal phase emulsion monoliths for the chromatographic separation of engineered nanoparticles. *J. Appl. Polym. Sci.* **2015**, *132*. [CrossRef]

44. Nemtsec Ivan, V.; Tambasov Igor, A.; Ivanenko Alexander, A.; Zyryanov Victor, Y.A. Angle-resolved reflection spectroscopy of high-quality PMMA opal crystal. *Photonics Nanostruct.* **2018**, *28*, 37–44.

45. Lai, C.F.; Wang, Y.C. Colloidal photonic crystals containing silver nanoparticles with tunable structural colors. *Crystals* **2016**, *6*, 61. [CrossRef]

46. Padmanabhan, S.C.; McGrath, J.; Bardosova, M.; Pemble, M.E. A facile method for the synthesis of highly monodisperse silica@gold@silica core-shell-shell particles and their use in the fabrication of three-dimensional metallodielectric photonic crystals. *J. Mater. Chem.* **2012**, *22*, 11978–11987. [CrossRef]

47. Rastogi, V.; Melle, S.; Calderon, O.G.; García, A.A.; Marquez, M.; Velev, O.D. Synthesis of light-diffracting assemblies from microspheres and nanoparticles in droplets on a superhydrophobic surface. *Adv. Mater.* **2008**, *20*, 4263–4268. [CrossRef]

48. Sperling, M.; Gradzielski, M. Droplets, evaporation and a superhydrophobic surface: Simple tools for guiding colloidal particles into complex materials. *Gels* **2017**, *3*, 15. [CrossRef]

49. Lin, H.; Song, L.P.; Huang, Y.J.; Cheng, Q.; Yang, Y.P.; Guo, Z.Y.; Su, F.M.; Chen, T. Macroscopic Au@Pani core/shell nanoparticle superlattice monolayer film with dual-responsive plasmonic switches. *ACS Appl. Mater. Interfaces* **2020**, *12*, 11296–11304. [CrossRef]